MI-0033

TRANSITION CROSSING IN THE MAIN INJECTOR - ESME SIMULATION

S.A. BOGACZ

TRANSITION CROSSING IN THE MAIN INJECTOR – ESME SIMULATION

S.A. Bogacz

Accelerator Physics Department, Fermi National Accelerator Laboratory*,

P.O. Box 500, Batavia, IL 60510, USA.

August 1990

A longitudinal phase-space tracking code (ESME) is used to model transition crossing in the Main Injector. The simulation is aimed at various collective and single particle effects contributing to the longitudinal emittance blowup. Our model takes into account the longitudinal space-charge force (bunch length oscillation), the transverse space-charge (the Umstätter effect) and finally the dispersion of the momentum compaction factor (the Johnsen effect). As a result of this simulation one can separate relative strengths of the above mechanisms and study their individual effects on the longitudinal phase-space evolution, especially filamentation of the bunch and formation of "galaxy-like" patterns. Finally, a simple scheme of γ_t-jump is implemented. Comparison of both cases (slow and fast transition crossing) points out that the above scheme can be very useful in suppressing beam loss and the emittance blowup at transition.

* Operated by the Universities Research Association under contract with the U.S. Department of Energy

Introduction

This study is motivated by the longitudinal phase-space dilution effects induced by the transition crossing. Here we employ ESME[1] as an effective tool to simulate transition crossing in the Main Injector. One of the obvious advantages of the simulation compared to existing analytic formalisms, e.g. based on the Vlasov equation[2], is that it allows us to consider the collective effects in a self-consistent manner with respect to the changing accelerating conditions. Furthermore this scheme enables us to model nonlinearities of the longitudinal beam dynamics, which are usually not tractable analytically[3].

Implemented in the simulation are both intensity dependent coherent forces (the longitudinal and transverse space charge) and single-particle kinematic effects due to the explicit momentum offset dependence of the momentum compaction factor, α. Their individual contributions to the longitudinal emittance blowup across transition are studied here. The transition crossing time for the synchronous particle is identified as a zero synchrotron tune point on the history plot, Fig. 1.

Longitudinal Phase Space Tracking with the Space Charge

The tracking procedure used in ESME consists of turn-by-turn iteration of a pair of Hamilton-like difference equations describing synchrotron oscillation in θ–ε phase-space ($0 \le \theta \le 2\pi$ for the whole ring and $\varepsilon = E - E_o$, where E_o is the synchronous particle energy). Knowing the particle distribution in the azimuthal direction, $\rho(\theta)$, and the revolution frequency, ω_o, after each turn, one can construct the longitudinal wake field induced by the coherent space charge force[4]

$$V_i(\theta) = e\omega_o \sum_{n=-\infty}^{\infty} \rho_n Z_{s\text{-}c}(n\omega_o) e^{in\theta},$$

where (1)

$$Z_{s\text{-}c}(n\omega_o) = \frac{nZ_o}{2\beta\gamma^2} \left\{ 1 + 2\ln\frac{b}{a} \right\} .$$

Here, a and b are the radii of the beam and the smooth vacuum pipe, respectively.

The above force is defocusing below and focusing above the transition. Therefore it corrects the equilibrium bunch length to be longer below and shorter above the transition (compare to the case without any space charge). This yields bunch length oscillation above the transition set off by nonlinear bunch length overshoot[5]. This phenomenon can be clearly observed by looking at the history of θ_{rms} or simply by watching "mountain range" evolution of the azimuthal bunch profile (see Figs. 7 and 12).

Implementation of the Umstätter and Johnson Effects, γ_t-jump Scheme

As a result of the transverse space charge forces each particle suffers a horizontal betatron tune shift, which is proportional to the particle density, $\rho(\theta)$, at the given longitudinal position θ. This tune shift translates directly into the change of γ_t. Close to the transition, when η goes through zero, even very small corrections to γ_t play dominant role and they govern the longitudinal beam dynamics. One of the features of ESME code is that each particle has its own γ_t, which allows us for straightforward implementation of the Umstätter effect (described above). Similarly, to account for the dispersion of the momentum compaction factor (Johnsen effect), different parts of the bunch (particles with different momentum offset) are allowed to cross transition at different times. Both contributions to the γ_t shift are summarized below[6]

$$\Delta\left(\frac{1}{\gamma_t}\right)^2 = 2hr_p R \frac{1}{\beta^2\gamma^7 a^2}\rho(\theta) - \alpha_1 \frac{\Delta p}{p} - 2j(t)\frac{1}{\gamma^3} \tag{2}$$

The last term in the above equation represents some external γ_t-jump accomplished by firing a pulsed quadrupole magnet. One purposely taylors j(t), so that the transition crossing happens much faster and no significant emittance blowup has time to develop. For the purpose of this simulation the last γ_t ma-

nipulation is implemented according to a simple η-program presented in Fig. 2. Here the rate of transition crossing is boosted by the factor of four (see Fig. 2)

ESME Simulation

As a starting point for our simulation a single bucket in θ–ε phase-space is populated with 5000 macro-particles according to a bi-Gaussian distribution matched to the bucket so that 95% of the beam is confined within the contour of the longitudinal emittance of 0.4 eV–sec. Each macro-particle is assigned an effective charge to simulate a bunch intensity of 6×10^{10} protons.

The first set of results, Fig.3-7, corresponds to the situation when only intensity dependent coherent forces are present ($\alpha_1 = 0$). The simulation is carried out over a symmetric (with respect to the transition) time interval of 2700 turns. Fig. 3 represents a sequence of the longitudinal phase space snap-shots taken every 400 turns. One can clearly see dilutions effects leading to extensive filamentation of the beam at transition. Fig. 4 illustrates longitudinal emittance blowup (100%) and beam loss (5%) at transition. The same characteristics for faster transition crossing are collected for comparison in Figs. 5 and 6. Here the emittance blowup reaches only 12% with no beam loss.

To visualize the position and shape of individual bunches as they evolve in time one can compose a "mountain range" diagram[4] by plotting θ-projections of the bunch density in equal increments of revolution number and then stacking the projections to imitate the time flow. The resulting mountain range plots for both cases are compared in Fig. 7.

The second set of simulations incorporates in addition to previously discussed coherent space charge forces also the Johnsen effect. The dispersion of the momentum compaction factor, α_1, is assigned a value of 5×10^{-3} and all three features described by Eqs. (1) and (2) are used in the simulation. Again, the phase-space snap shots, Figs. 8 and 9, refer to slower transition crossing, while Figs. 10 and 11 describe the scenario with γ_t-jump. Figs. 8 and 9 illustrate catastrophic beam loss at transition (50% loss); one can see very sharp tails made of particles rapidly steaming out of the bucket to the unstable region of the phase-

space. When the γ_t-jump is applied (see Figs. 10 and 11) the development of tails is much slower and the transition is successfully crossed with about 75% emittance blowout and about 6% beam loss. Finally, the mountain range plots for the case without and with the γ_t-jump (labeled by A and B) are summarized in Fig.12.

Conclusions

One can see from our simulation that the presence of large α_1 has crucial impact on beam degradation at transition. One can look at the Johnsen effect using simple physical picture of instantaneous phase space configurations. Particle with large positive momentum offset cross transition sooner than the synchronous particle and they end up "seeing" unstable phase-space region long before the synchronous phase is "snapped" ($\phi_s \rightarrow \pi - \phi_s$ at the transition crossing for the synchronous particle). They follow unstable orbits in phase space and eventually leave the bucket (long tail formation). Similarly, for particles with large negative momentum offset transition crossing is delayed with respect to the synchronous particle. After the synchronous phase "snap" they are still below transition and drifting into unstable region, which contributes to formation of the second tail (see Figs. 3, 5, 8 and 10). However by speeding up the transition crossing one can easily recover from substantial emittance blowup and beam loss. Therefore the γ_t-jump scheme should be given serious consideration in the context of Main Injector lattice design.

References

[1] J.A. MacLachlan, FERMILAB TM-1274 (1984)

[2] S. Krinsky and J.M. Wang, Particle Accelerators, **17**, 109 (1985)

[3] S. Stahl and S.A. Bogacz, Phys. Rev. D, **37**, 1300 (1988)

[4] J.A. MacLachlan, FERMILAB FN-446 (1987)

[5] S.A. Bogacz and K-Y Ng, Phys. Rev. D, **36**, 1538 (1987)

[6] A. S ørenssen, Particle Accelerators, **6**, 141 (1975)

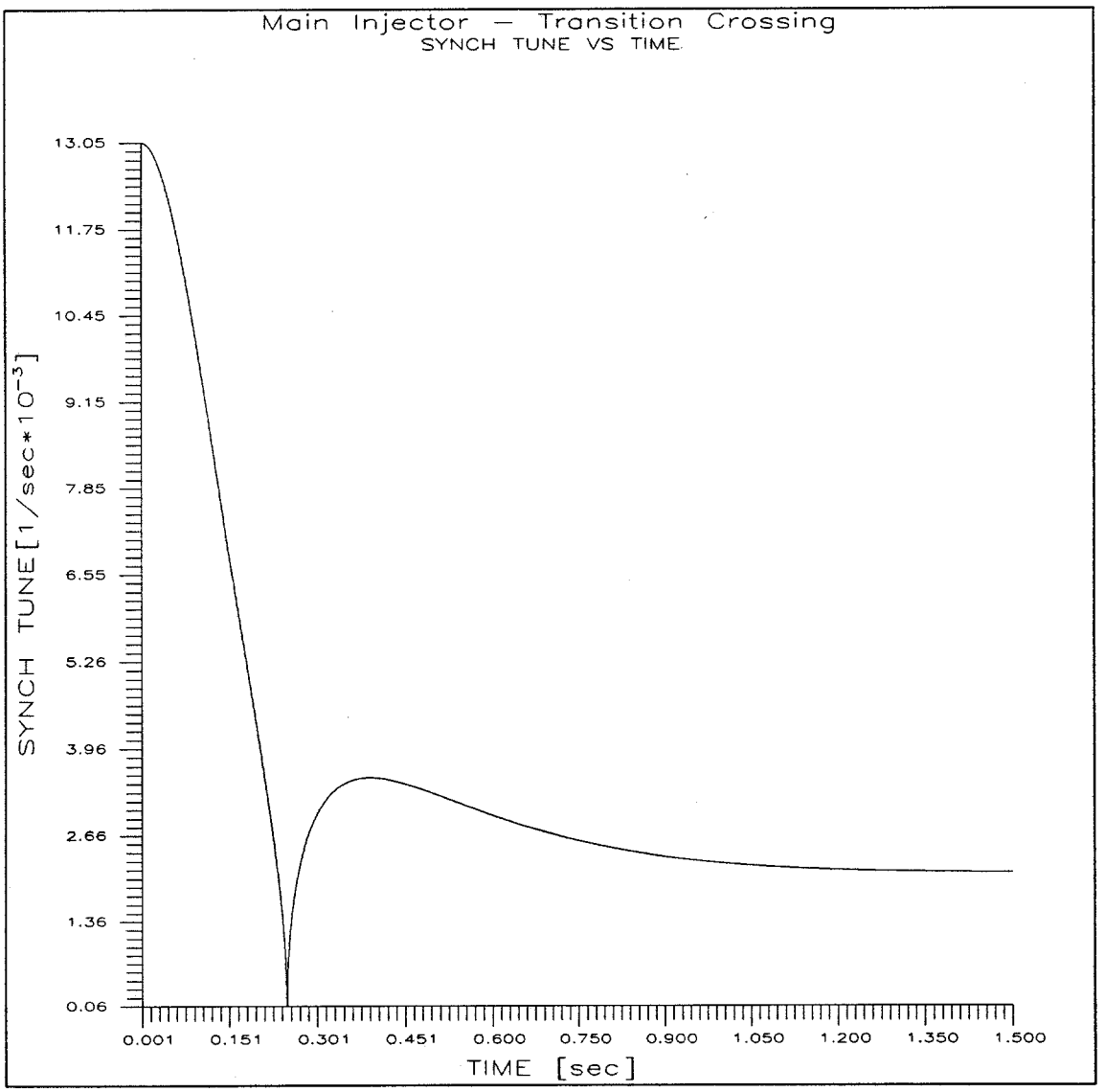
Main Injector — Transition Crossing
SYNCH TUNE VS TIME
SYNCH TUNE [1/sec*10^-3]
13.05
11.75
10.45
9.15
7.85
6.55
5.26
3.96
2.66
1.36
0.06
0.001
0.151
0.301
0.451
0.600
0.750
0.900
1.050
1.200
1.350
1.500
TIME [sec]

Fig. 1

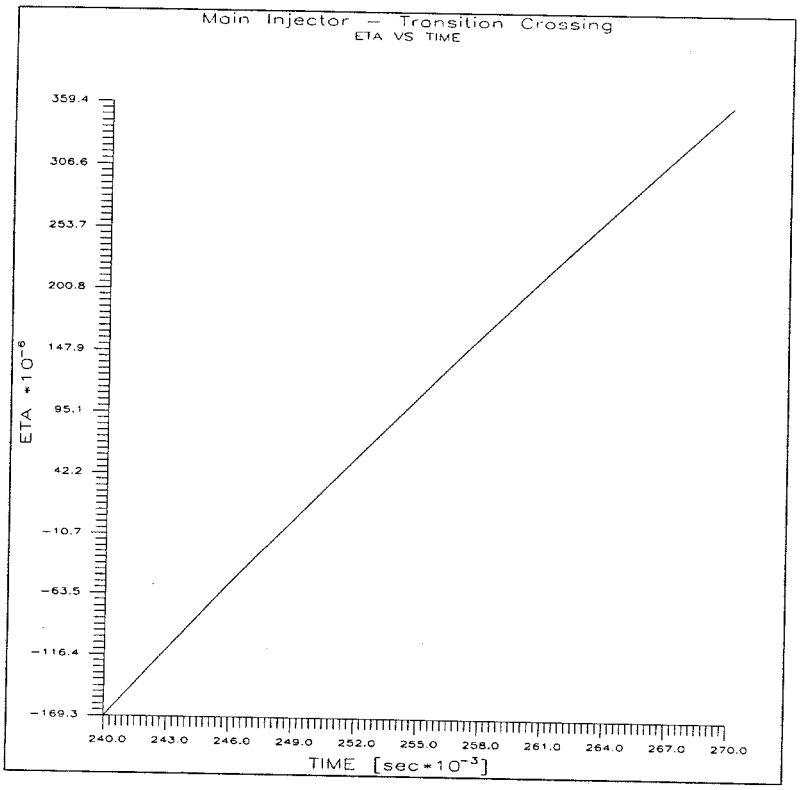
Main Injector – Transition Crossing
ETA VS TIME
359.4
306.6
253.7
200.8
147.9
95.1
42.2
-10.7
-63.5
-116.4
-169.3
ETA *10^-6
240.0
243.0
246.0
249.0
252.0
255.0
258.0
261.0
264.0
267.0
270.0
TIME [sec*10^-3]

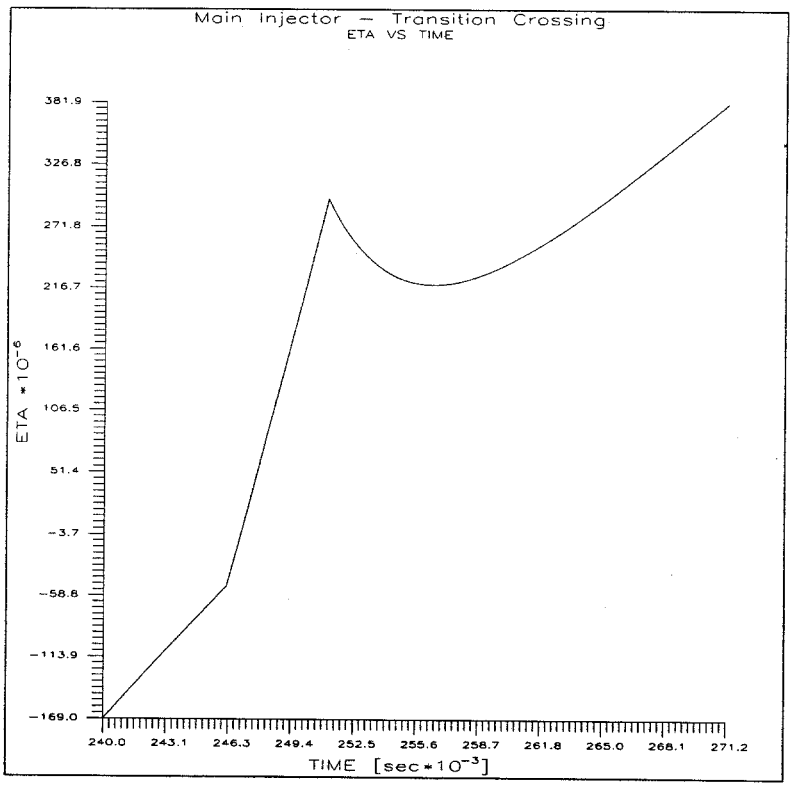
Main Injector – Transition Crossing
ETA VS TIME
381.9
326.8
271.8
216.7
161.6
106.5
51.4
-3.7
-58.8
-113.9
-169.0
ETA *10^-6
240.0
243.1
246.3
249.4
252.5
255.6
258.7
261.8
265.0
268.1
271.2
TIME [sec*10^-3]

Fig. 2

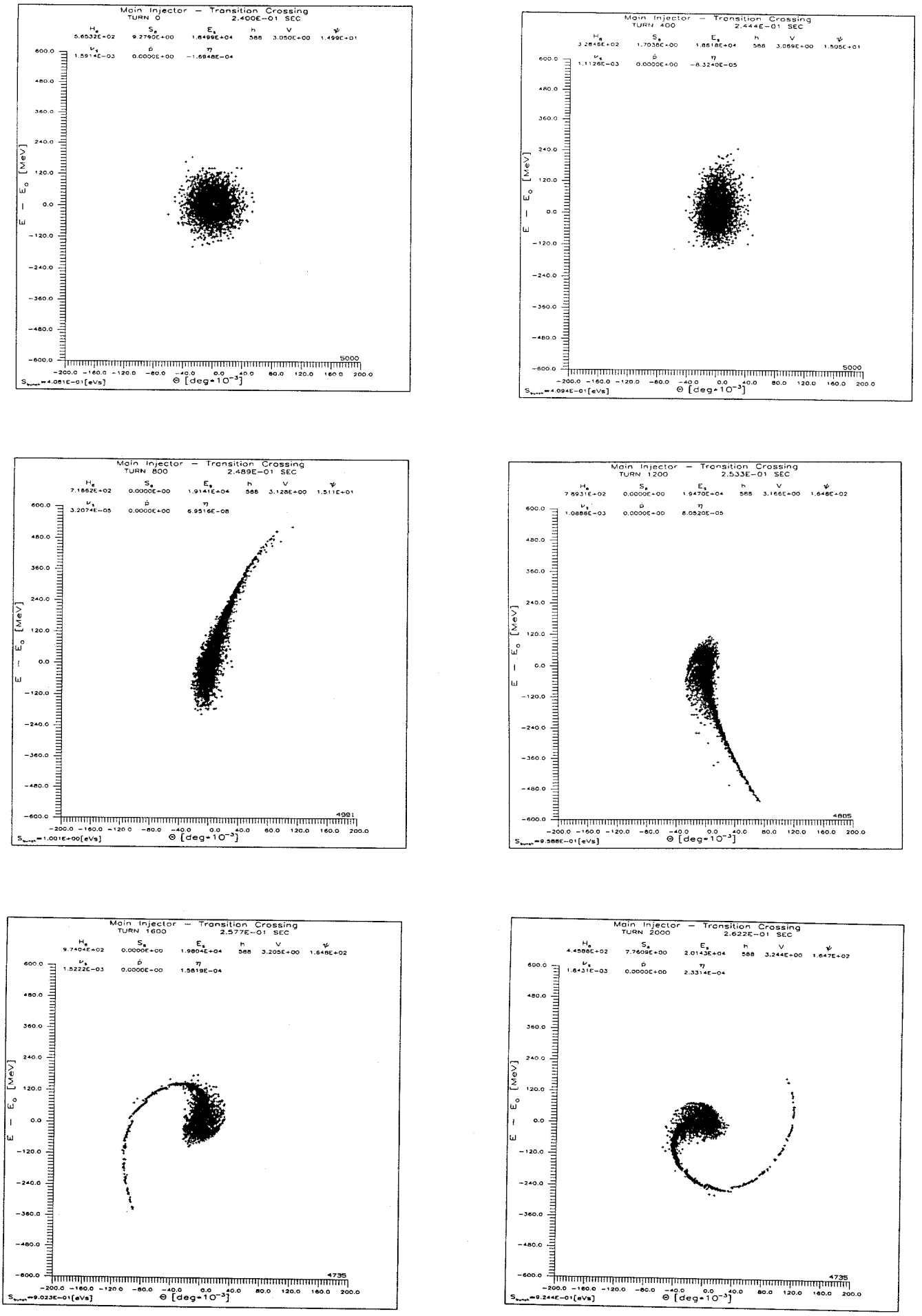
Main Injector – Transition Crossing
TURN 0 2.400E-01 SEC
Main Injector – Transition Crossing
TURN 400 2.444E-01 SEC
Main Injector – Transition Crossing
TURN 800 2.489E-01 SEC
Main Injector – Transition Crossing
TURN 1200 2.533E-01 SEC
Main Injector – Transition Crossing
TURN 1600 2.577E-01 SEC
Main Injector – Transition Crossing
TURN 2000 2.622E-01 SEC
E – E0 [MeV]
Θ [deg*10^-3]

Fig. 3

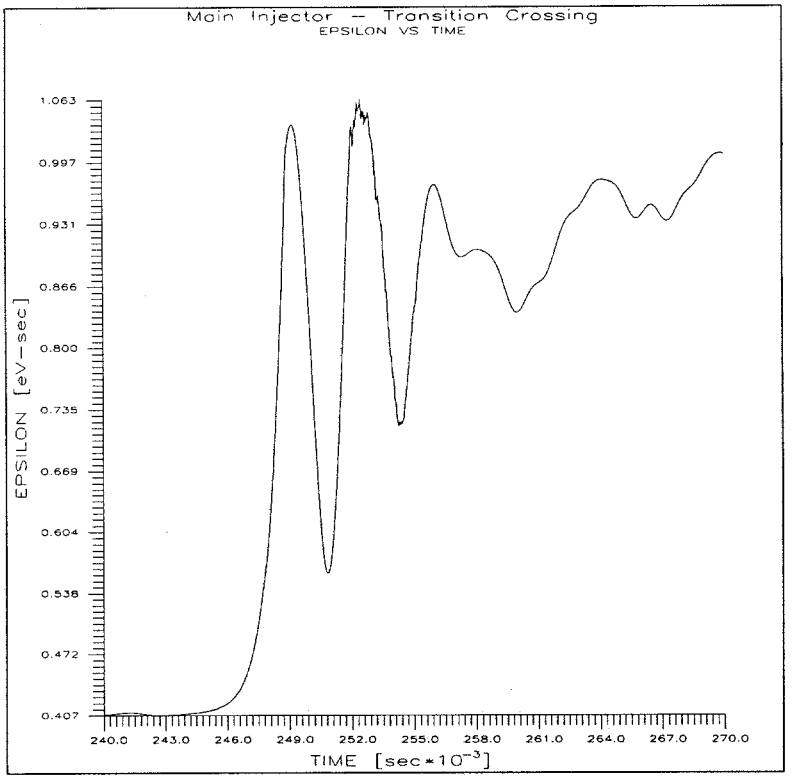
Main Injector – Transition Crossing
EPSILON VS TIME
EPSILON [eV–sec]
1.063
0.997
0.931
0.866
0.800
0.735
0.669
0.604
0.538
0.472
0.407
240.0 243.0 246.0 249.0 252.0 255.0 258.0 261.0 264.0 267.0 270.0
TIME [sec*10^-3]

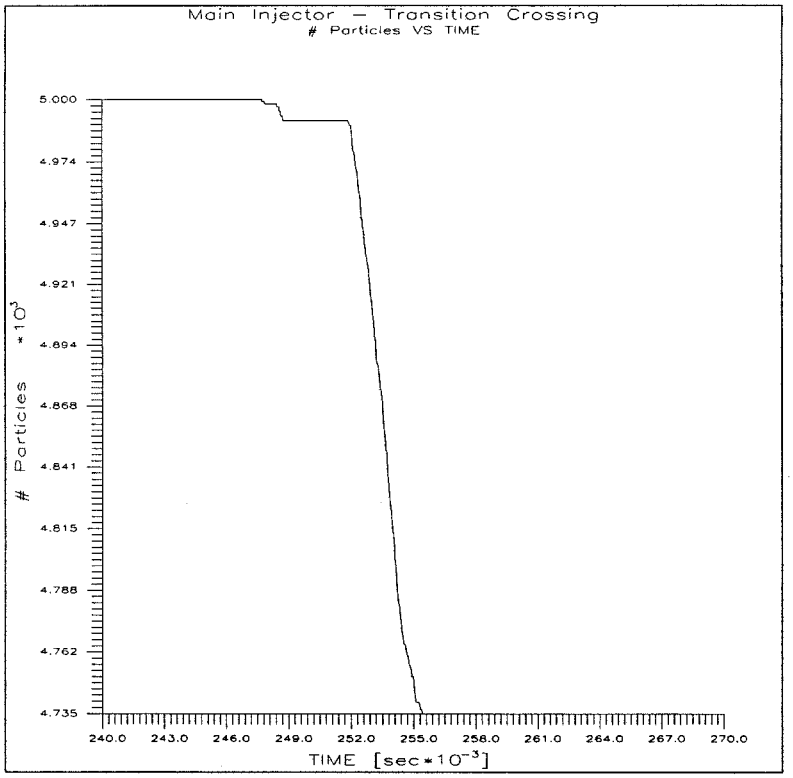
Main Injector – Transition Crossing
Particles VS TIME
Particles *10^3
5.000
4.974
4.947
4.921
4.894
4.868
4.841
4.815
4.788
4.762
4.735
240.0 243.0 246.0 249.0 252.0 255.0 258.0 261.0 264.0 267.0 270.0
TIME [sec*10^-3]

Fig. 4

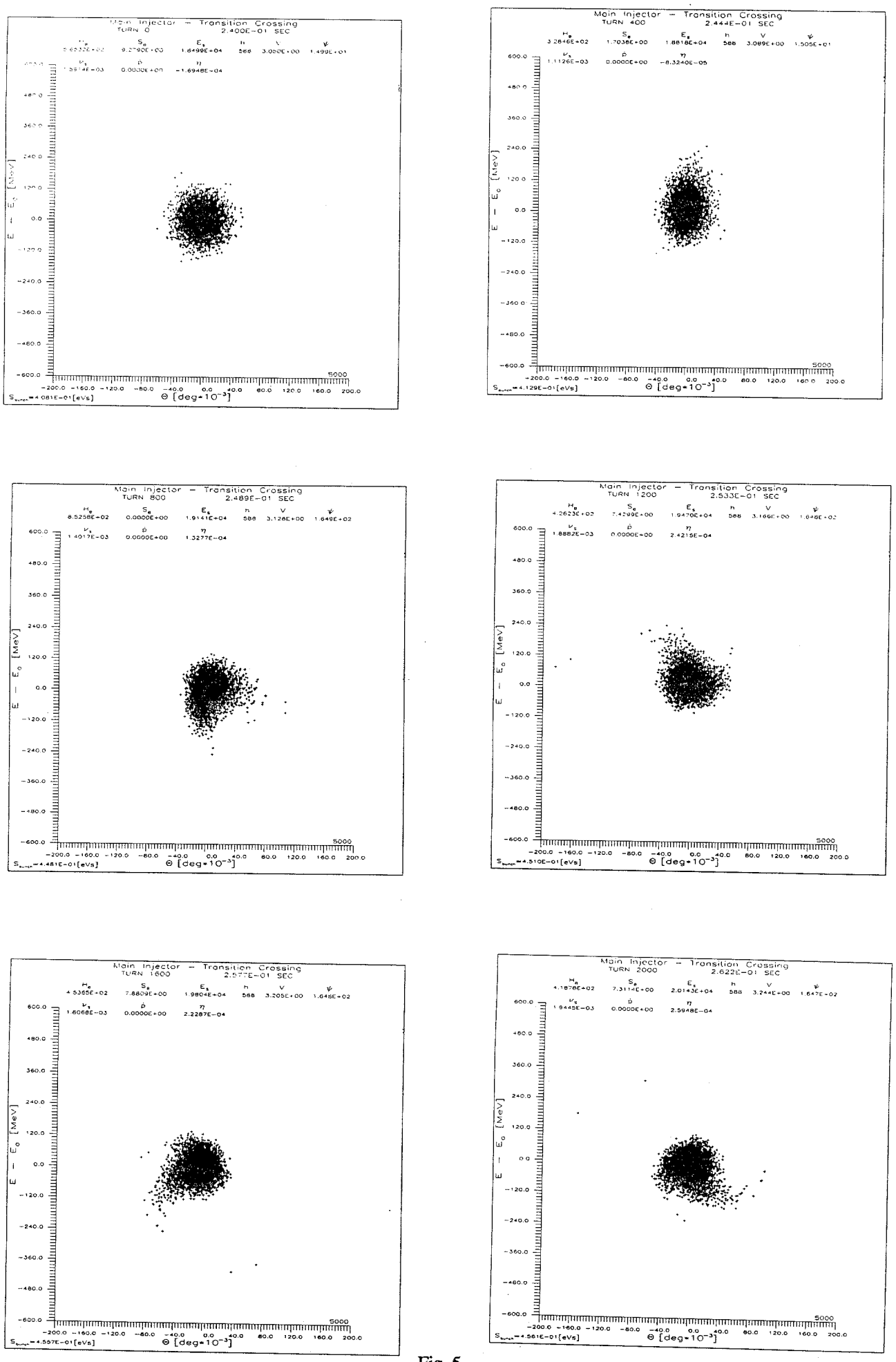
Main Injector – Transition Crossing
TURN 0 2.400E-01 SEC
Main Injector – Transition Crossing
TURN 400 2.444E-01 SEC
Main Injector – Transition Crossing
TURN 800 2.489E-01 SEC
Main Injector – Transition Crossing
TURN 1200 2.533E-01 SEC
Main Injector – Transition Crossing
TURN 1600 2.577E-01 SEC
Main Injector – Transition Crossing
TURN 2000 2.622E-01 SEC
E – E0 [MeV]
Θ [deg*10^-3]

Fig. 5

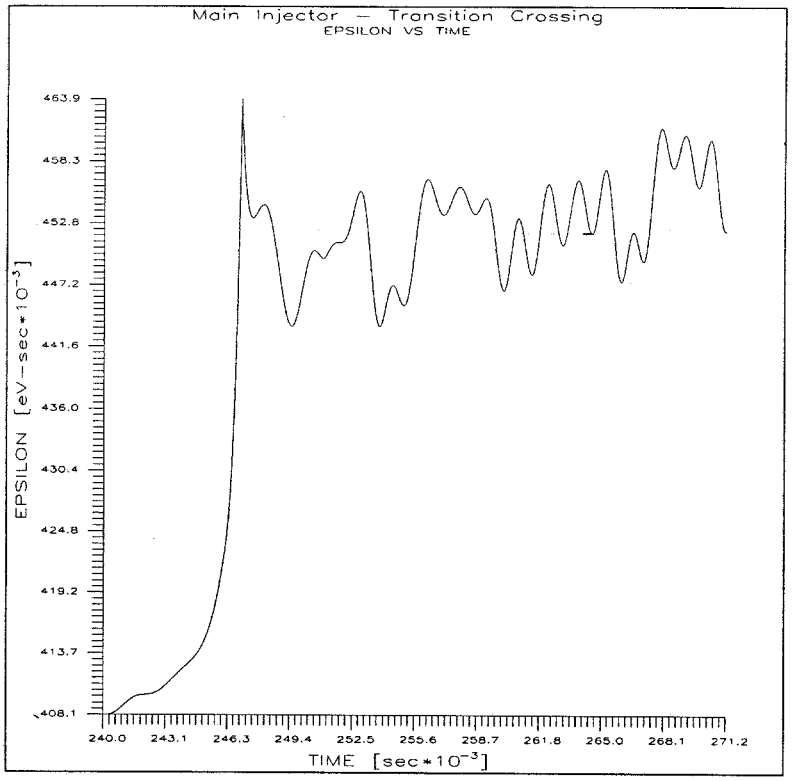
Main Injector – Transition Crossing
EPSILON VS TIME
EPSILON [eV–sec*10^-3]
463.9
458.3
452.8
447.2
441.6
436.0
430.4
424.8
419.2
413.7
408.1
240.0
243.1
246.3
249.4
252.5
255.6
258.7
261.8
265.0
268.1
271.2
TIME [sec*10^-3]

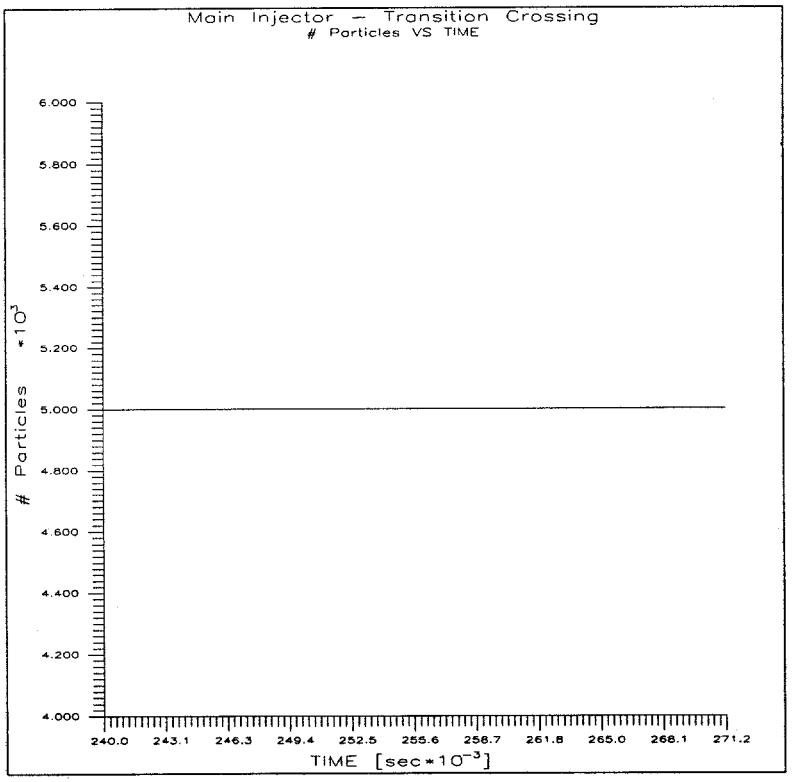
Main Injector – Transition Crossing
Particles VS TIME
Particles *10^3
6.000
5.800
5.600
5.400
5.200
5.000
4.800
4.600
4.400
4.200
4.000
240.0
243.1
246.3
249.4
252.5
255.6
258.7
261.8
265.0
268.1
271.2
TIME [sec*10^-3]

Fig. 6

A

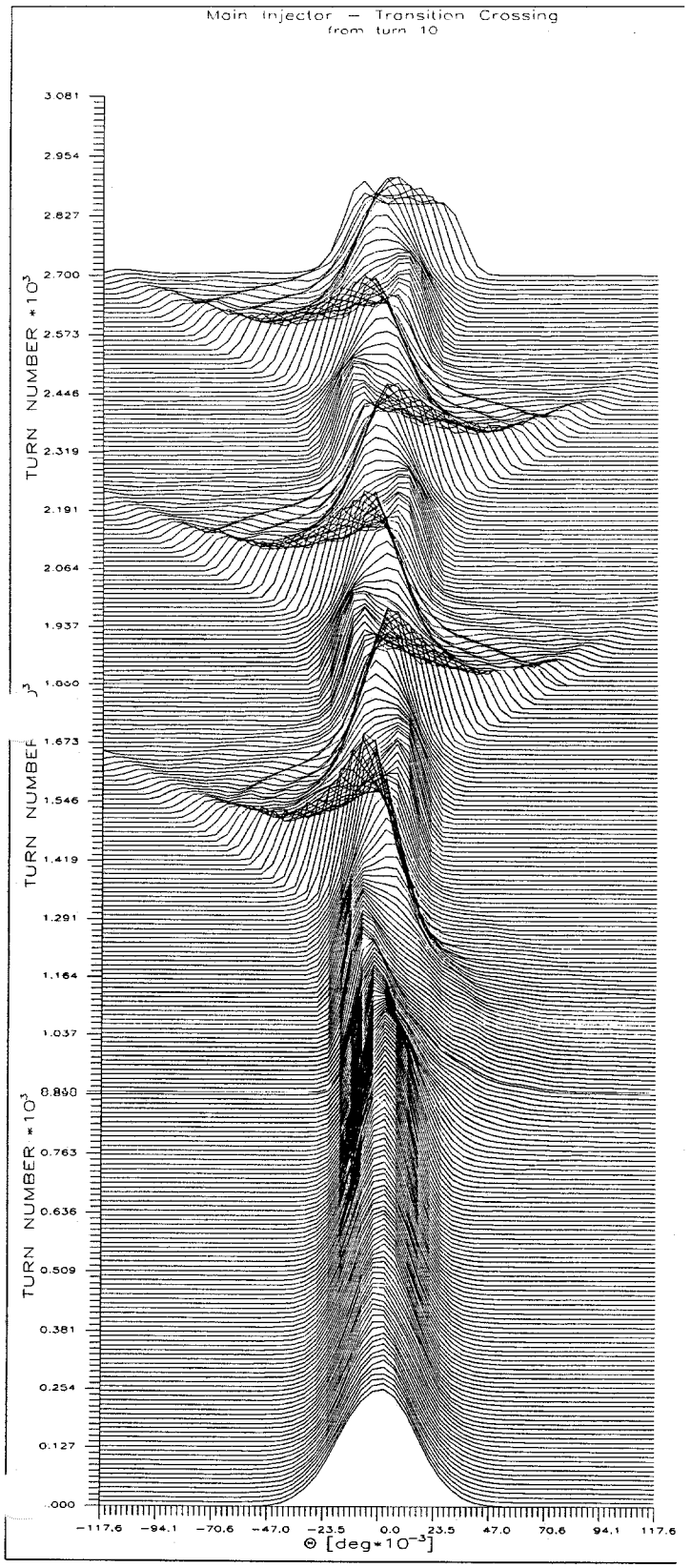
Main Injector – Transition Crossing
from turn 10
TURN NUMBER *10^3
3.081
2.954
2.827
2.700
2.573
2.446
2.319
2.191
2.064
1.937
1.673
1.546
1.419
1.291
1.164
1.037
0.763
0.636
0.509
0.381
0.254
0.127
.000
−117.6 −94.1 −70.6 −47.0 −23.5 0.0 23.5 47.0 70.6 94.1 117.6
Θ [deg*10^-3]

B

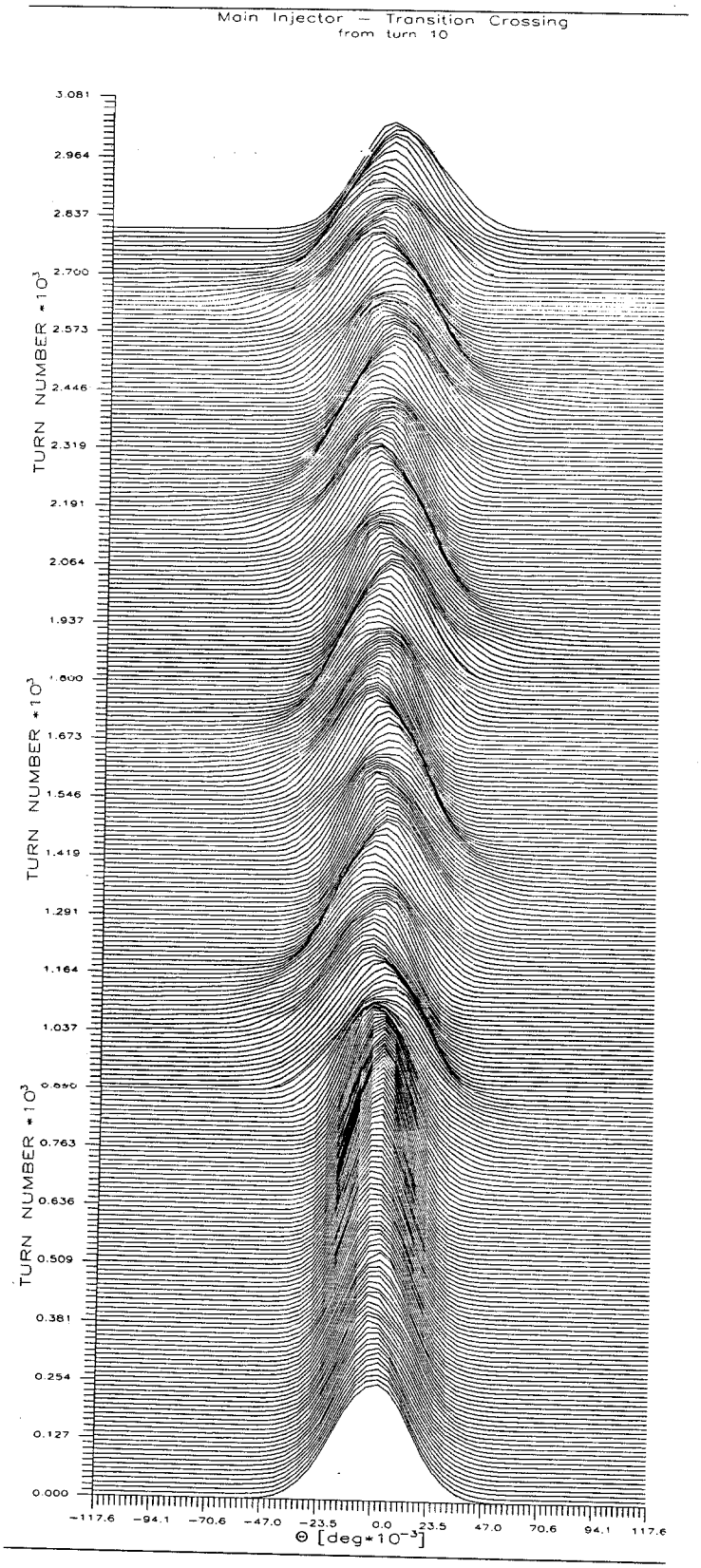
Main Injector – Transition Crossing
from turn 10
TURN NUMBER *10^3
3.081
2.964
2.837
2.700
2.573
2.446
2.319
2.191
2.064
1.937
1.673
1.546
1.419
1.291
1.164
1.037
0.763
0.636
0.509
0.381
0.254
0.127
0.000
−117.6 −94.1 −70.6 −47.0 −23.5 0.0 23.5 47.0 70.6 94.1 117.6
Θ [deg*10^-3]

Fig. 7

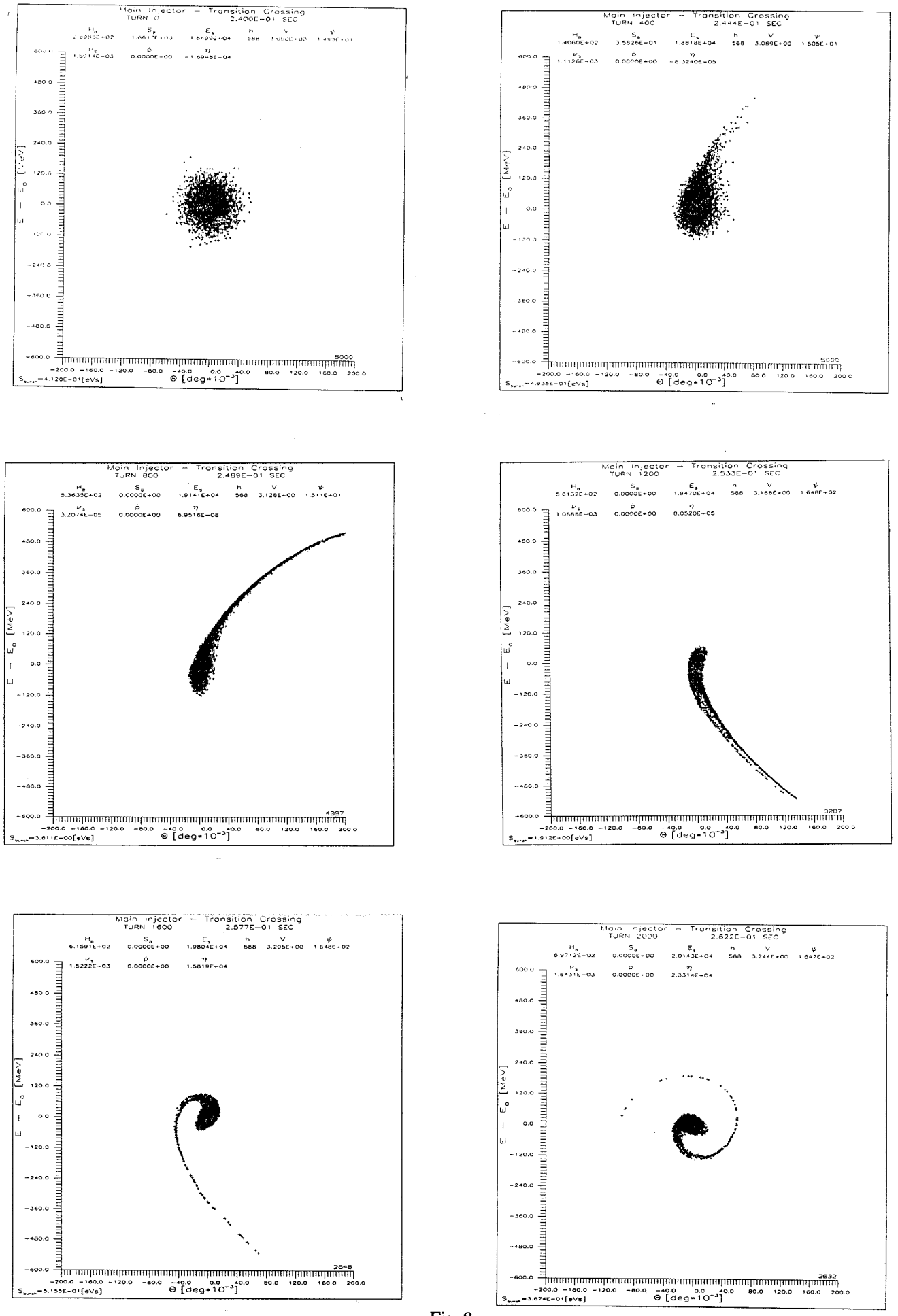
Main Injector – Transition Crossing
TURN 0 2.400E-01 SEC
Main Injector – Transition Crossing
TURN 400 2.444E-01 SEC
Main Injector – Transition Crossing
TURN 800 2.489E-01 SEC
Main Injector – Transition Crossing
TURN 1200 2.533E-01 SEC
Main Injector – Transition Crossing
TURN 1600 2.577E-01 SEC
Main Injector – Transition Crossing
TURN 2000 2.622E-01 SEC
E – E0 [MeV]
Θ [deg*10^-3]

Fig. 8

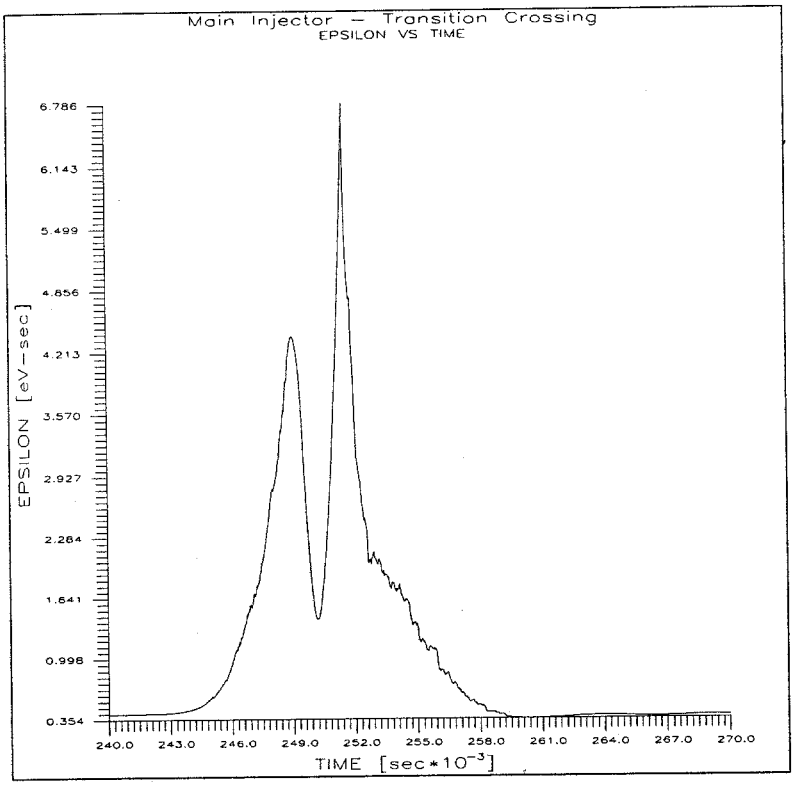
Main Injector – Transition Crossing
EPSILON VS TIME
EPSILON [eV-sec]
6.786
6.143
5.499
4.856
4.213
3.570
2.927
2.284
1.641
0.998
0.354
240.0
243.0
246.0
249.0
252.0
255.0
258.0
261.0
264.0
267.0
270.0
TIME [sec*10^-3]

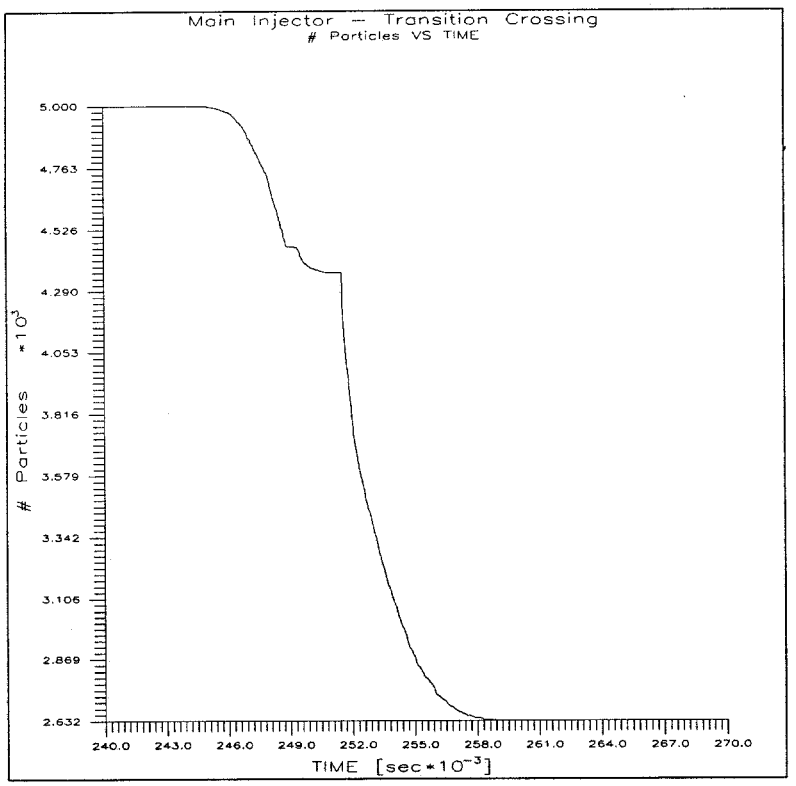
Main Injector – Transition Crossing
Particles VS TIME
Particles *10^3
5.000
4.763
4.526
4.290
4.053
3.816
3.579
3.342
3.106
2.869
2.632
240.0
243.0
246.0
249.0
252.0
255.0
258.0
261.0
264.0
267.0
270.0
TIME [sec*10^-3]

Fig. 9

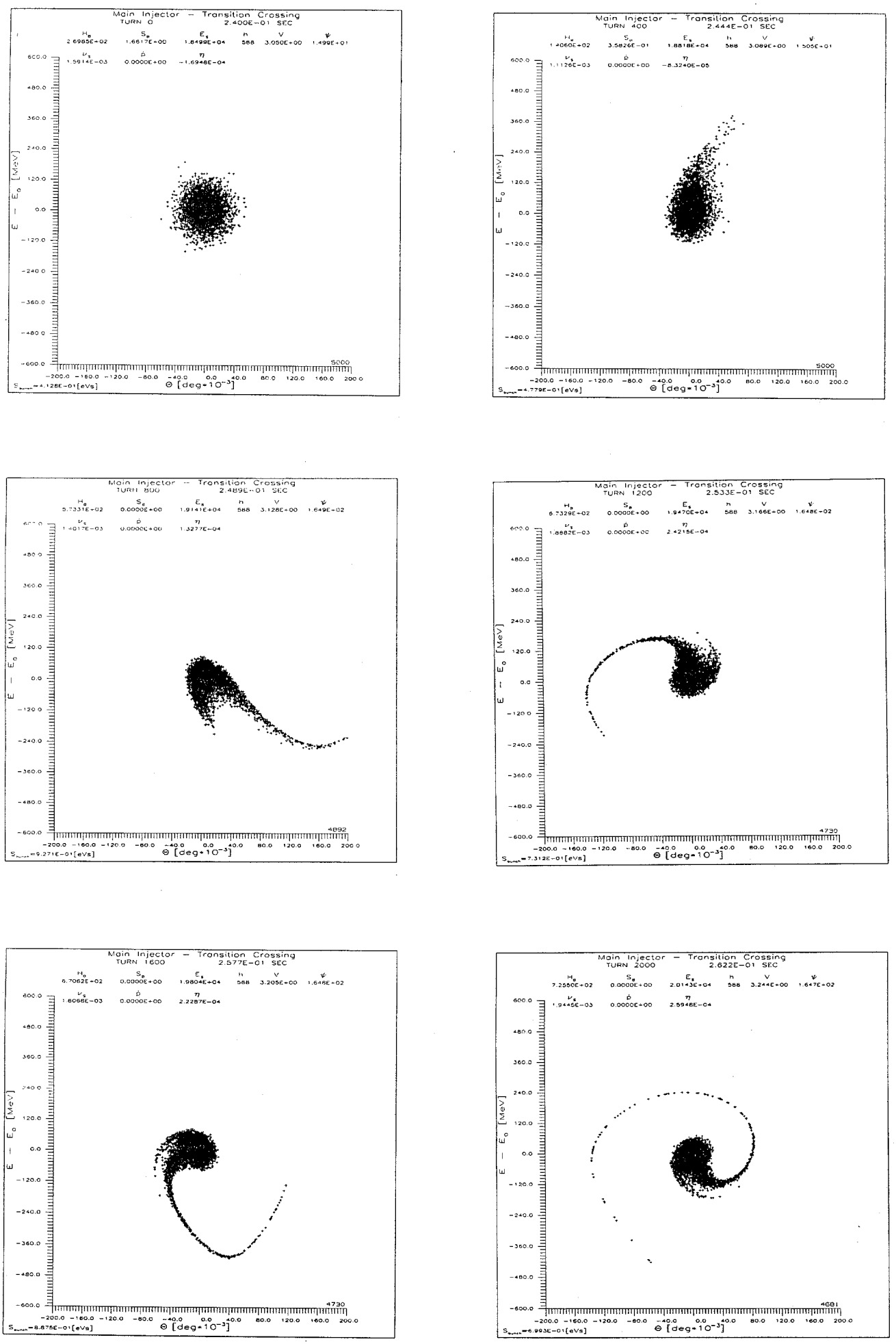
Main Injector – Transition Crossing
TURN 0
2.400E-01 SEC
Main Injector – Transition Crossing
TURN 400
2.444E-01 SEC
Main Injector – Transition Crossing
TURN 800
2.489E-01 SEC
Main Injector – Transition Crossing
TURN 1200
2.533E-01 SEC
Main Injector – Transition Crossing
TURN 1600
2.577E-01 SEC
Main Injector – Transition Crossing
TURN 2000
2.622E-01 SEC
E – E0 [MeV]
Θ [deg*10^-3]

Fig. 10

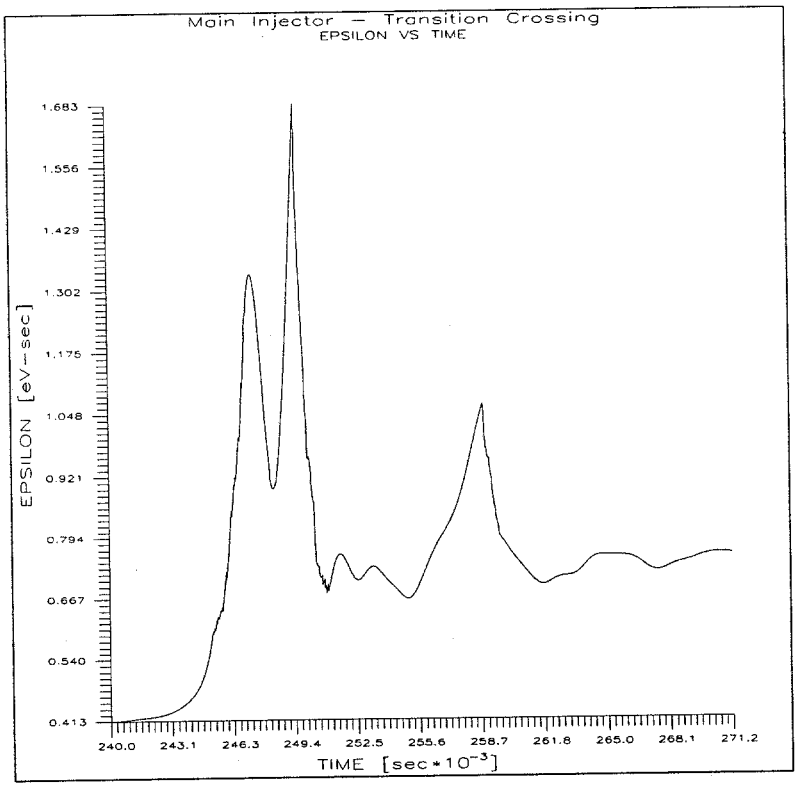
Main Injector – Transition Crossing
EPSILON VS TIME
EPSILON [eV–sec]
1.683
1.556
1.429
1.302
1.175
1.048
0.921
0.794
0.667
0.540
0.413
240.0
243.1
246.3
249.4
252.5
255.6
258.7
261.8
265.0
268.1
271.2
TIME [sec*10^-3]

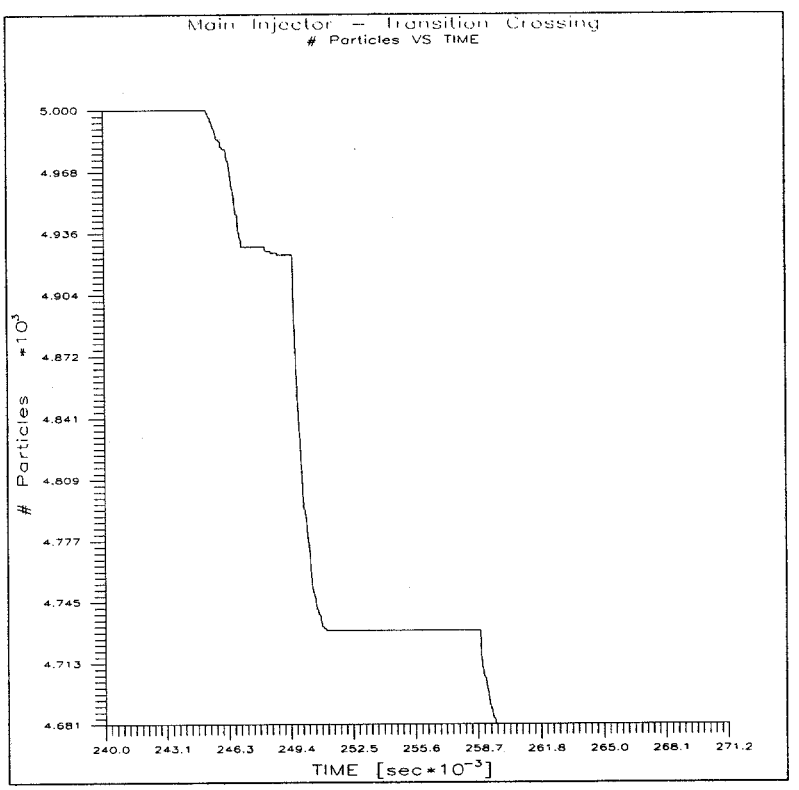
Main Injector – Transition Crossing
Particles VS TIME
Particles *10^3
5.000
4.968
4.936
4.904
4.872
4.841
4.809
4.777
4.745
4.713
4.681
240.0
243.1
246.3
249.4
252.5
255.6
258.7
261.8
265.0
268.1
271.2
TIME [sec*10^-3]

Fig. 11

A

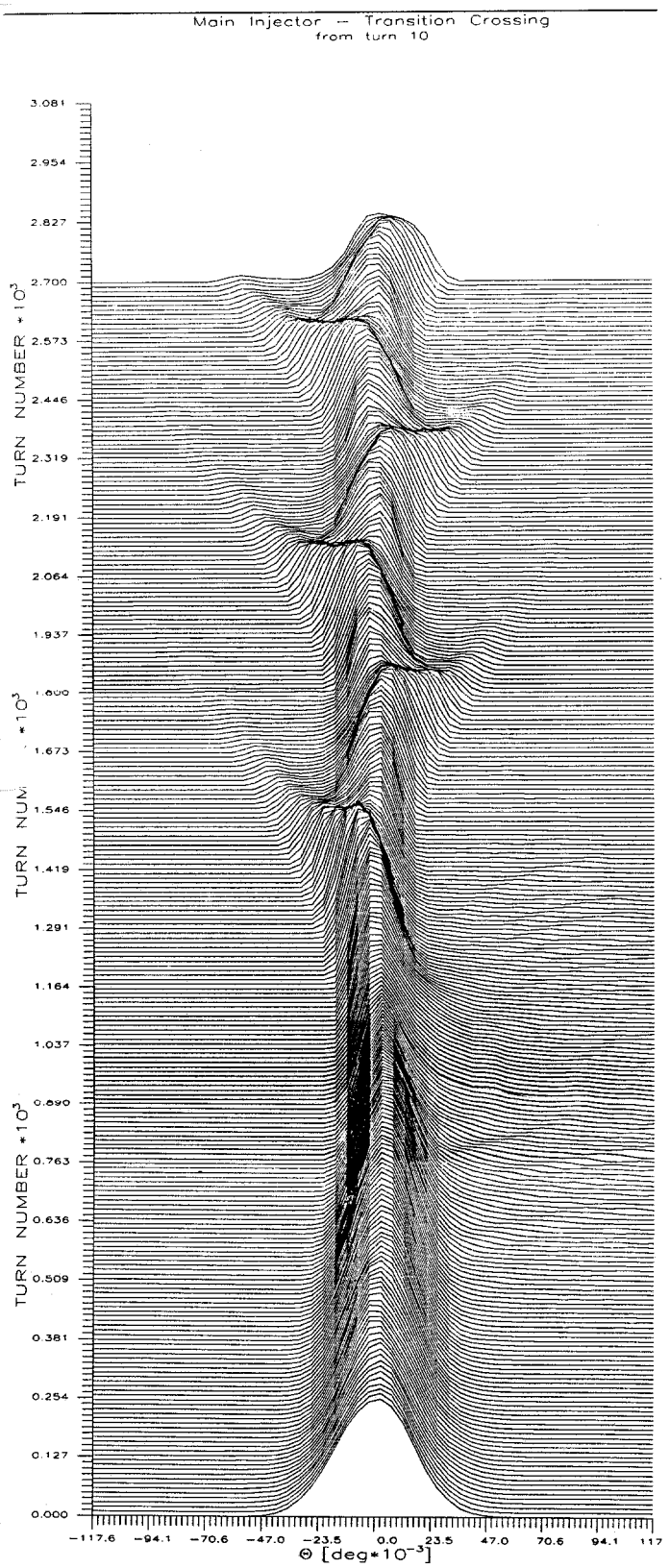
Main Injector -- Transition Crossing
from turn 10
TURN NUMBER *10^3
3.081
2.954
2.827
2.700
2.573
2.446
2.319
2.191
2.064
1.937
1.673
1.546
1.419
1.291
1.164
1.037
0.890
0.763
0.636
0.509
0.381
0.254
0.127
0.000
-117.6 -94.1 -70.6 -47.0 -23.5 0.0 23.5 47.0 70.6 94.1 117
Θ [deg*10^-3]

B

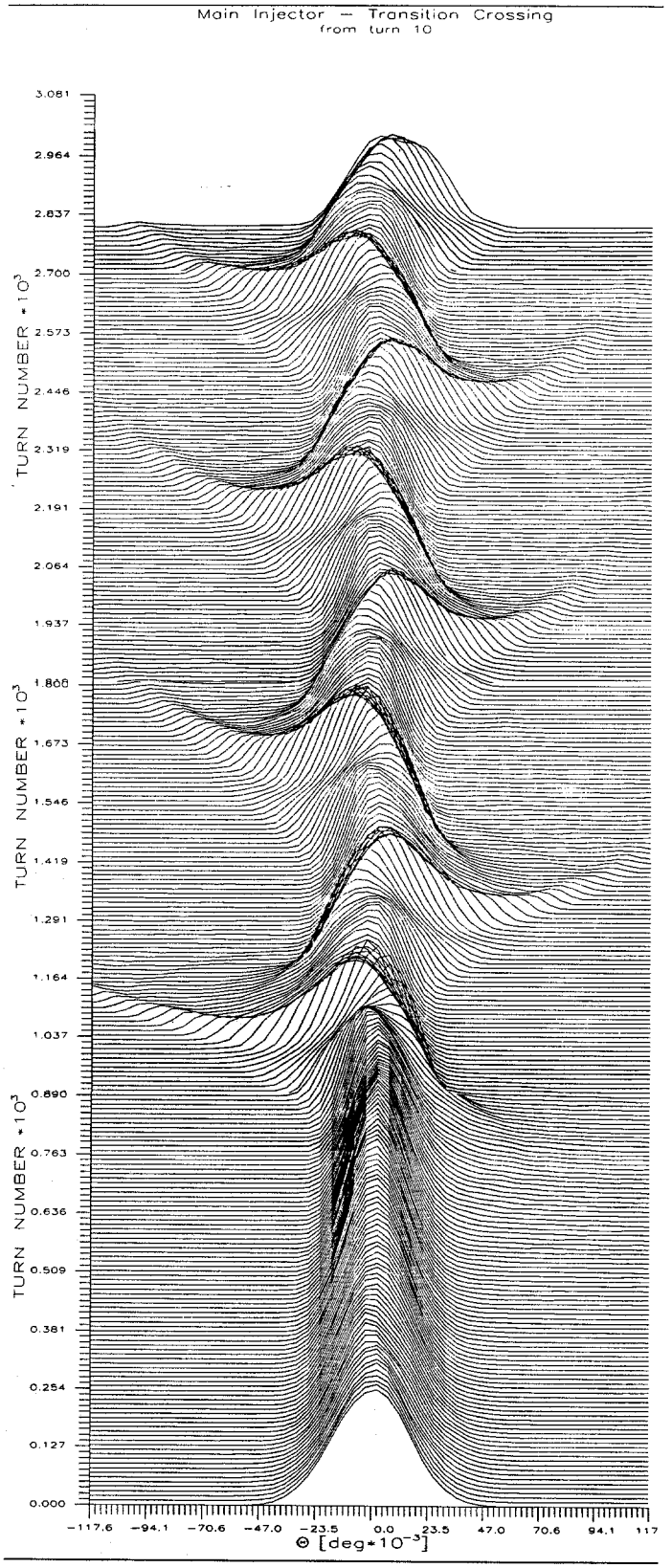
Main Injector -- Transition Crossing
from turn 10
TURN NUMBER *10^3
3.081
2.964
2.837
2.700
2.573
2.446
2.319
2.191
2.064
1.937
1.808
1.673
1.546
1.419
1.291
1.164
1.037
0.890
0.763
0.636
0.509
0.381
0.254
0.127
0.000
-117.6 -94.1 -70.6 -47.0 -23.5 0.0 23.5 47.0 70.6 94.1 117
Θ [deg*10^-3]

Fig. 12